Available online at www.sciencedirect.com
SCIENCE DIRECT
Bioorganic & Medicinal Chemistry 14 (2006) 1743–1749
Bioorganic & Medicinal Chemistry

Ribonucleic guanidine demonstrates an unexpected marked preference for complementary DNA rather than RNA

Myunji Park, Joseph W. Toporowski and Thomas C. Bruice*

Department of Chemistry and Biochemistry, University of California at Santa Barbara, CA 93106, USA

Received 8 October 2005; accepted 14 October 2005
Available online 8 November 2005

Abstract—Replacement of the phosphodiester linkages of DNA and RNA by guanidinium linkages provides DNG and RNG. We report here the order of stability of mixed duplexes (RNG-U_5·DNA-A_5 ≫ RNA-U_5·RNA-A_5 > RNG-U_5·RNA-A_5 > RNA-U_5·DNA-A_5 > DNA-T_5·DNA-A_5). The considerable stability of RNG·DNA compared to RNG·RNA is shown to be due to the rigid backbone of RNG existing only in B-form and therefore lowering its affinity for A-RNA. RNG oligomers are putative antigene agents which are specific for DNA and would have minimal competitive binding to ncRNA.

1. Introduction

The possible therapeutic use of oligonucleotide analogs as effective gene regulatory agents in antisense and antigene approaches has kindled interest in their development.[1–5] Key goals in the design of such agents include increased binding affinity while maintaining sequence specificity, resistance to degradation by cellular nucleases, and improved membrane permeability. Rapid degradation of natural oligonucleotides' phosphodiester backbones by cellular nucleases necessitated the creation of chemically modified oligonucleotides. Oligonucleotides connected by methylphosphonate,[6,7] methylenemethylimino (MMI),[8] and amide linkages[9] are representative of this strategy. An alternative approach involves replacing the sugar-phosphate backbone entirely, such as in the case of peptide nucleic acid (PNA),[10–12] phosphonic ester nucleic acid (PHONA),[13] and nucleic acid analog peptide (NAAP).[14] The modified backbones of these oligonucleotide analogs render them resistant to nuclease degradation.

To increase the free energy of oligonucleotide duplex formation, the negative charge–charge repulsion in DNA and RNA can be minimized or eliminated if the phosphodiester linkages are replaced by uncharged or positively charged linkages. Addressing these design features led us to develop deoxynucleic guanidine (DNG), which is generated via the replacement of the negative phosphodiester linkages of DNA [–O–(PO_2^-)–O–] with positively charged guanidinium linkages [–NH–C(=NH_2^+)–NH–].[15–17] This replacement alters the electrostatic nature between strands from being repulsive in native DNA duplexes to attractive in DNG·DNA duplexes. These favorable interactions lead to exceptional binding affinities accompanied by excellent specificities, ideal characteristics for a potential antisense agent.[18–21] In addition to these results, the guanidinium linkage was shown to be nuclease resistant,[22] and the positively charged backbones may give rise to increased cell membrane permeability via electrostatic attraction of the guanidine moieties to the negative phosphates on the cell surface.

The susceptibility of RNA to nuclease hydrolysis limits its application as an antigene/antisense agent and as a therapeutic tool such as RNAi, its susceptibility to various nucleases and the labile nature of the phosphodiester backbone limit its application.[23] To overcome those shortcomings, efforts to develop stable RNA mimics are needed. Ribonucleic guanidine (RNG, Fig. 1), wherein the negatively charged phosphodiester linkages of RNA have been replaced by positively charged guanidinium linkages, should be better suited as an antisense/antigene agent because the guanidinium linkages are neither susceptible to cellular nucleases nor chemical degradation under physiological conditions. We have reported the synthesis[24,25] and binding properties of

Keywords: Ribonucleic guanidine; Thermal denaturation; Circular dichroism; Molecular dynamics.
* Corresponding author. Tel.: +1 805 893 2044; fax: +1 805 893 2229; e-mail: tcbruice@chem.ucsb.edu

0968-0896/$ - see front matter © 2005 Elsevier Ltd. All rights reserved.
doi:10.1016/j.bmc.2005.10.028

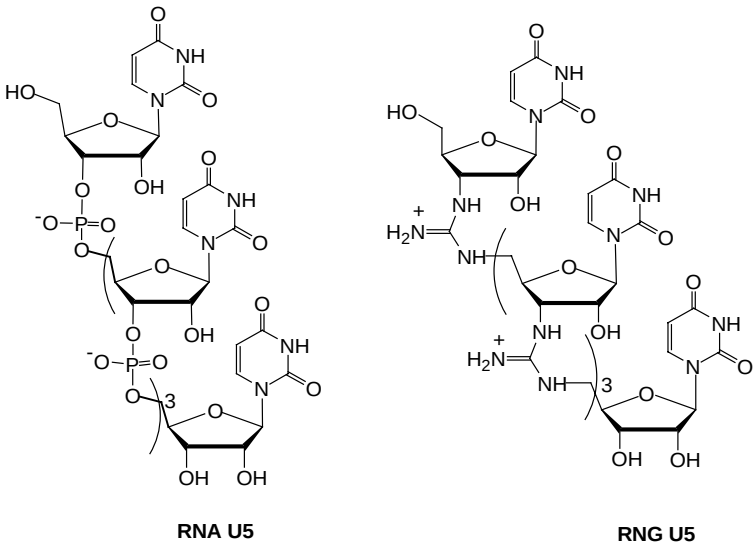

Figure 1. Structures of RNA-U_5 and RNG-U_5.

RNG to DNA.[26] A pentameric uridyl oligomer of RNG (RNG-U_5), with four positively charged guanidinium linkages, has been shown to bind to DNA-A_5 with unprecedented high affinity in a 1:1 uridyl/adenine complex. Interactions between RNG-U_5 with polyguanine, polycytidine, and polythymine were not observed, implying that RNG exhibits fidelity of base-pair recognition, discriminating between complementary and non-complementary base-pairs. At single mismatch points, stability decreased by approximately 7 °C, while no interactions were observed between RNG-U_5 and DNA oligomers with two or three mismatched bases.

Because the guanidinium modified oligomers bind so tightly to DNA, it was necessary to work with short strands to study the melting and annealing properties. In fact, pentameric duplex RNG-U_5·DNA-A_5 has a T_m value of 62 °C,[26] and longer strands (7–8 mers and above) are not expected to melt in boiling water. Ideally, one would want to compare the modified and native duplexes of a strand length that demonstrates clear melting transitions for both analogs.

Circular dichroism (CD) spectra of duplexes RNG-U_5·DNA-A_5 and DNA-T_5·DNA-A_5 showed positive bands around 275 nm and negative bands around 245 nm that are attributable to B-DNA-like conformations. This result is in agreement with that of molecular modeling,[27] which predicted that the overall structure of RNG is equilibrated as a B-DNA conformation, and the RNG strand adopts the general conformation of the DNA backbone. The loss in CD band intensity in RNG-U_5·DNA-A_5 compared to that in DNA-T_5·DNA-A_5 results from particular RNG backbone torsion angles differing from those of standard A-RNA values. These variances relieve the tension due to the replacement of the phosphodiester linkage with the guanidinium linkage. The remarkable degree of binding stability and specificity of RNG to DNA, as well as the characteristic global conformation of the RNG-U_5·DNA-A_5 duplex, led us to explore the following binding studies of RNG to RNA.

We report here the RNG-U_5 binding properties to RNA. We find that in comparison to the RNA-U_5·RNA-A_5 duplex, RNG-U_5 forms a surprisingly unstable complex with RNA-A_5. Results of CD and molecular dynamics (MD) of a RNG-U_5·RNA-A_5 duplex have been examined in order to investigate the destabilizing factors inherent in the duplex. It is pointed out that the preference of RNG for DNA may have advantages in antigene therapy.

2. Results and discussion

2.1. Stoichiometry of binding

The binding stoichiometry of RNG-U_5 and DNA-A_5 was determined by the continuous variation method[28] to generate mixing curves of the absorbance versus mole fraction of RNG-U_5 and RNA-A_5 (Fig. 2). This method is based on the assumption that a decrease in absor-

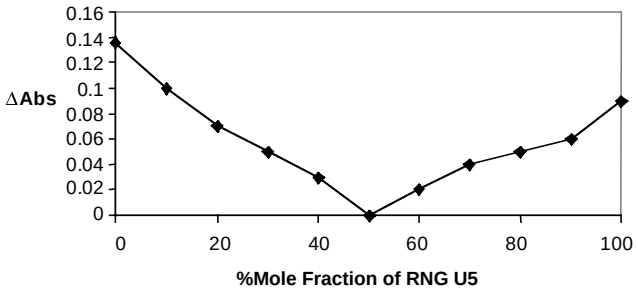

Figure 2. Job plot[28] mixing curves of the absorbance change at 260 nm (ΔA_{260}) of aqueous solutions (pH 7.0, $\mu = 0.12$ at 20 °C) with varied mole fractions of RNG-U_5 and DNA-A_5 ([RNG-U_5] + [RNA-A_5] = 2.0 μM). The inflection point indicates the stoichiometry to be a RNG·RNA duplex.

bance is proportional to the number of base-pairs that are hydrogen bonded between interacting species. Increasing the mole fraction of RNG-U_5 to RNA-A_5 (pH 7.0 and $\mu = 0.10$ with KCl at 20 °C) lowered the UV absorbance at 260 nm. An inflection point at 0.5 mole fraction indicated the formation of a RNG-U_5·RNA-A_5 duplex with the expected 1:1 stoichiometry.

2.2. Melting studies

The stabilities of the duplexes formed from RNG-U_5 and RNA-A_5 were studied by thermal denaturation experiments. To confirm the effect of the guanidinium linkage of the RNG on the thermal stability of the duplexes, the T_m values for unmodified RNA-U_5·RNA-A_5, RNA-U_5·DNA-A_5, and DNA-T_5·DNA-A_5 duplexes were also determined. Unexpectedly, the RNG-U_5·RNA-A_5 duplex was less stable than the RNA-U_5·RNA-A_5 duplex. As shown in Figure 3, the order of thermal stability was: RNG-U_5·DNA-A_5 > RNA-U_5·RNA-A_5 > RNG-U_5·RNA-A_5 > RNA-U_5·DNA-A_5 > DNA-T_5·DNA-A_5. The cooling curves of each of the duplexes exhibited hysteresis, indicating that the RNG·RNA complex is not held together purely by electrostatic attractions. Although there is no considerable difference thermodynamically between the RNG-U_5·RNA-A_5 and RNA-U_5·RNA-A_5 duplexes,[26,29–31] it is a surprising outcome in that replacement of the negative phosphates with positive guanidiniums was expected to increase the binding affinity by reversing the electrostatic repulsions that exist in a RNA-U_5·RNA-A_5 duplex (Fig. 3).

The free energy ($\Delta G° = -11.2$ kcal/mol) for the formation of the RNG-U_5·DNA-A_5 duplex has been determined by use of the van't Hoff calculation method. To have some comparison of the RNG-U_5·RNA-A_5 binding energy with that of RNG-U_5·DNA-A_5, we used regression analysis to obtain an approximate RNG-U_5·RNA-A_5 T_m of ~3 °C and very approximate free energies. We surmise that $\Delta\Delta G°$ is somewhere in the vicinity of 4 kcal/mol such that the equilibrium constant for RNG-U_5·DNA-A_5 formation exceeds that for RNG-U_5·RNA-A_5 formation by possibly 10^3.

2.3. Circular dichroism spectra

It has been observed that the effect of phosphorothioate backbone modifications led to decreases in T_m values of complexes formed from such oligomers (S-d$(AC)_{12}$·r$(GU)_{12}$ and r$(AC)_{12}$·S-d$(GT)_{12}$). Such sulfur modifications of oligonucleotide duplexes also caused pronounced effects on CD spectra.[32,33] To assess the effects of the guanidinium modification on the conformation of the RNG·RNA structures, duplexes of RNG-U_5 with RNA-A_5 were characterized using CD spectrometry.

The CD spectra of the single strands in Figure 4 show significant differences between RNG-U_5 and unmodified RNA-U_5 and DNA-T_5. The CD sign difference demonstrates that RNG-U_5 must exist in a stacked conformation that is quite different from those of unmodified RNA and DNA.[34,35] CD spectra of the RNA-A_5 and DNA-A_5 duplexes with RNG-U_5 are shown in Figure 5. The CD spectrum of the RNA-U_5·RNA-A_5 duplex has negative bands at 300 nm and below 210 nm, and a positive band at 260 nm characteristic of an A-RNA conformation (Fig. 5A).[34,36,37] The spectrum of the DNA-T_5·DNA-A_5 duplex has roughly equal positive and negative bands above 240 nm, with a crossover at 260 nm typical of a B-conformation (Fig. 5B).[35,38] The CD spectrum of the duplex formed from RNG-U_5 and the DNA-A_5 exhibits B-form characteristics similar to those of the control (DNA-T_5·DNA-A_5) oligonucleotide (Fig. 5B).[26] However, the CD spectrum of the RNG-U_5·RNA-A_5 duplex differs from those of both RNA-U_5·RNA-A_5 (reference A-form) and DNA-T_5·DNA-A_5 (reference B-form) (Figs. 5A and B). The RNG-U_5·RNA-A_5 spectrum shows a large decrease in band magnitudes and does not show the first crossover at 260 nm. These differences may imply changes in torsion angles around the guanidinium group of the RNG-U_5 strand and in the winding angle for RNA-A_5 duplexed with RNG-U_5.[38] Based on these results, the destabilizing effect of the guanidinium substitution appears to come

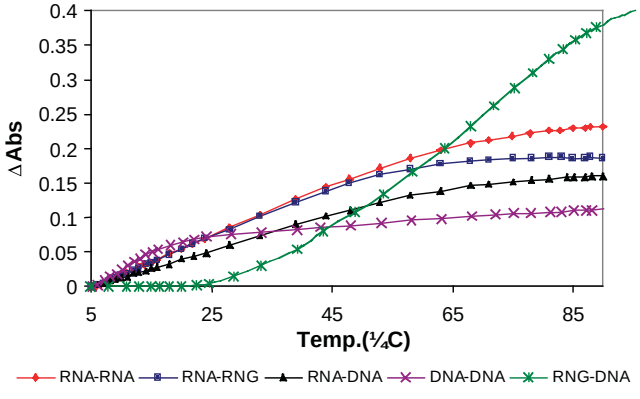

Figure 3. Thermal denaturation curves for RNG and complementary RNA and DNA, and unmodified RNA and DNA duplexes. Absorbance was measured at 260 nm, [oligomer] = 4 μM, [K_2HPO_4] = 10 mM, [KCl] = 100 mM, pH 7.0.

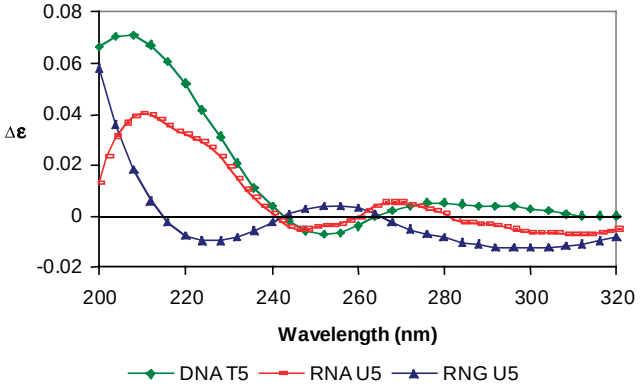

Figure 4. CD spectra of a RNG-U_5 single strand compared of RNA-U_5 and DNA-T_5 single strands. [oligomer] = 4 μM, [K_2HPO_4] = 10 mM, [KCl] = 100 mM, pH 7.0.

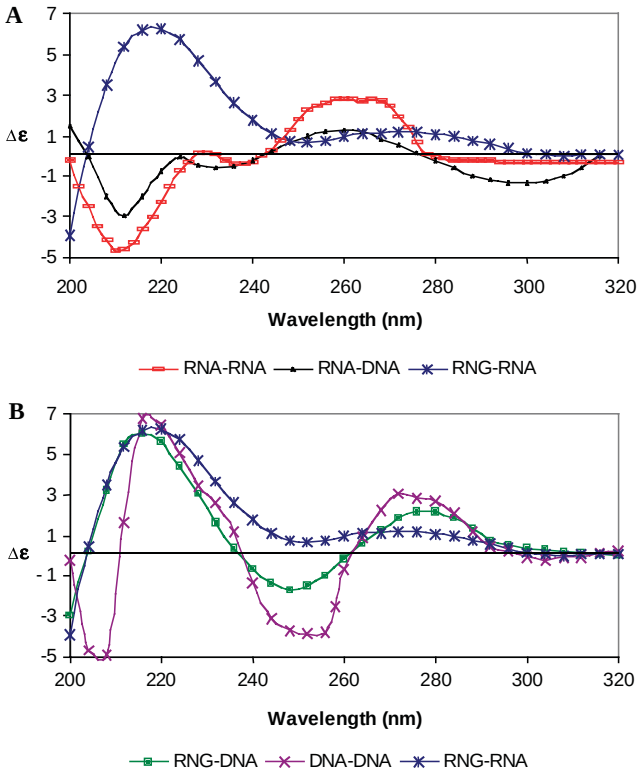

Figure 5. (A) CD spectra of RNG-U_5·RNA-A_5 compared to those of RNA-U_5·RNA-A_5 and RNA-U_5·DNA-A_5 complex (reference A-form). (B) CD spectra of RNG-U_5·RNA-A_5 compared to those of DNA-T_5·DNA-A_5 and RNG-U_5·DNA-A_5 (reference B-form). [oligomer] = 4 μM, [K_2HPO_4] = 10 mM, [KCl] = 100 mM, pH 7.0.

from a conformational change upon forming the RNG-U_5·RNA-A_5 duplex. However, although structural changes cause the RNG-U_5·RNA-A_5 duplex to be less stable than RNA-U_5·RNA-A_5, it is more stable than RNA-U_5·DNA-A_5 which has standard A-form character (Fig. 5A). This reveals that electrostatic interactions between the positive guanidinium linkages and negative phosphodiester linkages still exist. To help further elucidate the conformation of the RNG·RNA helix and the lower than expected T_m values, the dodecamers RNG-U_{12}·RNA-A_{12} and RNA-U_{12}·RNA-A_{12} were modeled by use of 5 ns MD simulations.

2.4. MD simulations

The root-mean-square deviations (rmsd) for the MD simulations are given in Figure 6, and the simulations can be seen to converge within 1 ns. The rmsd of the RNG·RNA simulation compared to its minimized structure (3.04 ± 0.47 Å) is similar to the rmsd compared to canonical A-RNA (2.70 ± 0.41 Å), and canonical B-RNA is slightly higher (4.61 ± 0.58 Å). The RNA·RNA rmsd with respect to its minimized structure is 2.36 ± 0.55 Å.

The results of the MD simulations show the RNG-U_{12}·RNA-A_{12} duplex in an intermediate conformation between canonical A- and B-forms (Table 1). The sugar puckers for both strands adopt C3′-*endo* conformations (10 ± 8° for RNG-U_{12} and 13 ± 8° for RNA-A_{12}), typical of RNA and A-form polynucleotides. Glycosyl torsion χ is *anti* at 197 ± 7° for both strands, also characteristic of A-RNA. Despite these parameters being distinctive of A-form, several helical parameters lie between canonical forms (Table 1), including roll, rise, and inclination. The intrastrand phosphate–phosphate ($P_n \cdots P_{n+1}$) and guanidinium carbon–carbon ($C_n \cdots C_{n+1}$) distances vary between the strands, with the RNA values (6.0 ± 0.3 Å) being typical for A-form, while the RNG values (6.6 ± 0.2 Å) are similar to normal B-form of 6.8 Å.[39]

While many of the helical parameters are typical of canonical forms, the RNG·RNA duplex exhibits very large propeller values of −45 ± 9° (Figs. 7 and 8), compared with native RNA NMR values of −14 to −22°.[40] The large propeller values are believed to stem from the tendency of the RNG backbone to adopt more elongated structures versus the compact A-form usually observed in RNA. The sp^3 phosphate in the RNA backbone is very flexible, allowing for more compact structures, while the sp^2 hybridized guanidinium groups of RNG are rigid and locked in a planar conformation due to electron delocalization. The results of these flexibility differences can be seen in the intrastrand $P_n \cdots P_{n+1}$ and $C_n \cdots C_{n+1}$ distances. In the RNA·RNA simulation, the $P_n \cdots P_{n+1}$ distances are 5.9 ± 0.4 Å, normal for A-form. In the RNG·RNA simulation, the RNA strand $P_n \cdots P_{n+1}$ distance is similar at 6.0 ± 0.3 Å. However, the RNG strand is significantly longer at 6.6 ± 0.2 Å. To compensate for this difference in strand length, the RNG·RNA duplex exhibits large amounts of propeller, which has been suggested to reduce intrastrand clashes[41] and may help to maintain the fidelity of base-pair stacking. The propeller is significant enough to not only break the original O4 ··· N6 hydrogen bond, but to allow the RNG-U O4 atoms to hydrogen bond with the RNA-A N6 (via H62) atoms from the previous base-pair (Fig. 8), therefore partially compensating for the loss of the natural hydrogen bond. However, this alternative hydrogen bonding pattern is not expected to be as stable as the natural Watson–Crick

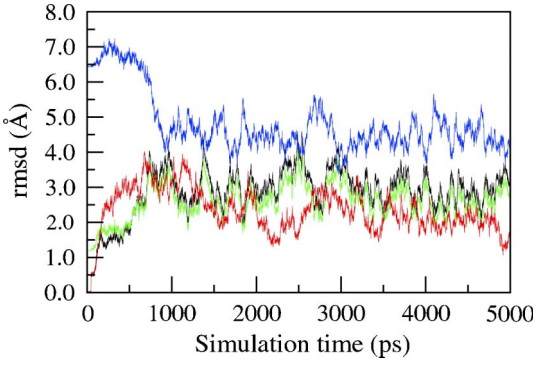

Figure 6. Time variation plots of the rmsd for RNG-U_{12}·RNA-A_{12} and RNA-U_{12}·RNA-A_{12}, including the RNG·RNA values with respect to the minimized structure (black), canonical A-form (green), and canonical B-form (blue), and the RNA·RNA duplex with respect to its minimized structure (red).

Table 1. Sugar pucker, glycosyl torsion χ, and helical parameters (with standard deviations) for the MD simulations of RNG-U_{12}·RNA-A_{12} and RNA-U_{12}·RNA-A_{12}

	RNG·RNA	RNA·RNA	A-form	B-form
Pucker (°)	C3′-*endo*	C3′-*endo*	C3′-*endo*	C2′-*endo*
χ (°)	197 ± 7	200 ± 8	199	252
Roll (°)	4 ± 8	8 ± 7	11	−3
Tilt (°)	−13 ± 4	−1 ± 3	1	0
Twist (°)	32 ± 3	30 ± 4	33	36
Rise (Å)	3.0 ± 0.3	2.5 ± 0.4	2.3	3.4
Slide (Å)	−1.1 ± 0.3	−1.8 ± 0.4	−1.6	−0.2
Tip (°)	25 ± 8	2 ± 6	−1	0
Inclination (°)	9 ± 5	18 ± 5	20	−5
Propeller (°)	−45 ± 9	−9 ± 8	11	−1
Buckle (°)	−7 ± 6	3 ± 11	0	0
X-disp. (Å)	−3.8 ± 0.8	−5.7 ± 1.1	−4.5	0.2

Parameters averaged over the last 4.5 ns for the central 8 base-pairs. Canonical data for helical parameters obtained by use of FREEHELIX[36] on structures generated with QUANTA98.[20]

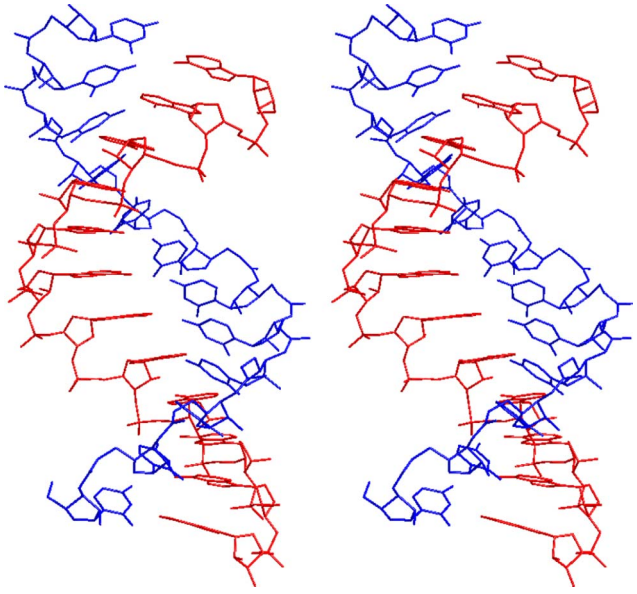

Figure 7. A stereo-view of the RNG-U_5·RNA-A_5 1–5 ns averaged structure with the RNG strand in blue and the RNA in red. The structure displays high levels of propeller, which are especially apparent in the center of this heavy-atom image.

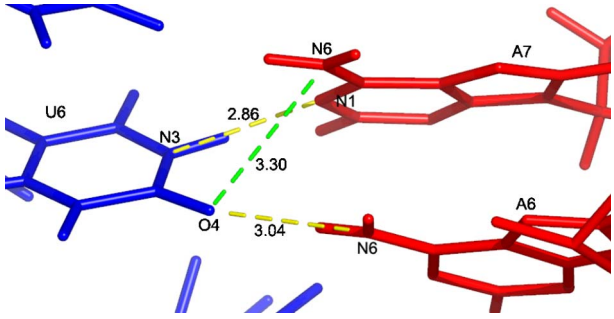

Figure 8. A close-up view of the RNG-U_5·RNA-A_5 1–5 ns averaged structure with RNG in blue and RNA in red. Relevant residues, atoms, and potential heavy-atom hydrogen bonding distances (Å) are labeled. Normally two hydrogen bonds would exist between U6 and A7 at atoms N3 ··· N1 and O4 ··· N6. The large amount of propeller causes the O4 ··· N6 hydrogen bond (shown in green) to break, and instead the O4 forms a hydrogen bond with the N6 of the previous nucleotide, in this case A6.

patterns. The modified hydrogen bonding network would increase the rigidity of the duplex, since each nucleotide is now bonded to two interstrand nucleotides, therefore lowering the entropy of the system.

3. Conclusions

Pentameric uridyl RNG binds to an adenyl RNA strand in a 1:1 ratio. Even though there is an electrostatic attraction in place of an electrostatic repulsion, a RNG·RNA complex is thermodynamically slightly disfavored in comparison to a RNA·RNA duplex. The CD spectra show that the instability of the RNG·RNA duplex results from the alteration of the natural conformation of RNA upon forming a duplex with RNG. In contrast, these results also demonstrate that the sustained B-type DNA conformation of the RNG·DNA duplex has contributed to increase the stability of the duplex via electrostatic attraction.[14] Molecular dynamics suggests that the different functional groups of the RNG·RNA backbone lead to differences in backbone flexibility and length. The duplex compensates for these differences by adopting high levels of base-pair propeller, which in turn causes the natural U-O4 ··· A-N6 hydrogen bond to break. The propeller leaves the U-O4 atom in position to hydrogen bond with the A-N6 atom of the previous base-pair.

From the order of thermal stabilities of the five mixed pairs composed of RNA-A_5, RNG-U_5, DNA-A_5, and DNA-T_5, the RNG-U_5·DNA-A_5 is clearly the most stable, while DNA-T_5·DNA-A_5 is the least stable. The rigid B-form of RNG means it will be specific for B-DNA and cannot bind tightly to A-form oligonucleotides. Thus, RNG markedly differentiates between complementary RNA and DNA. RNG sequences compatible with the DNA transcriptional start sites may serve to protect from TF-proten·DNA complex formation and, thus,

gene silencing. Unwanted RNG complexing to ncRNA[42] would not compete.

4. Experimental

4.1. Stoichiometry of binding

The stoichiometry of binding was determined by the method of continuous variations. Solutions ([RNG-U_5] + [RNA-A_5] = 2.0 M) containing different molar ratios of RNG-U_5 and RNA-A_5 were heated to 90 °C and allowed to cool slowly to 15 °C. The pH was maintained at 7.0 with 10 mM K_2HPO_4 buffer, while the ionic strength was held constant at 100 mM KCl. The absorbance of each solution at 260 nm (15 °C) was measured with a Cary 100-E2 9802310Z UV/Vis spectrometer. RNA and DNA oligomer concentrations were determined spectrophotometrically using extinction coefficients provided by the manufacturer (Integrated DNA Technologies). The extinction coefficient value of RNA-U_5 (ε_{260} = 48,700 M^{-1} cm^{-1}) was used for that of RNG-U_5. The reported absorbances are averages of three experiments (±0.01).

4.2. Melting studies

Thermal denaturation (T_m) measurements were obtained by observing the absorbances at 260 nm of a solution of oligomers in 1 cm path-length quartz cuvettes as the temperature was raised 0.5 °C/min from 5 to 90 °C. All samples had been previously annealed by cooling from 90 to 5 °C and stored at 5 °C overnight. Samples consisted of 2 μM RNG-U_5 and 2 μM RNA-A_5 with 10 mM K_2HPO_4 buffer at pH 7.0 and μ = 0.100 with KCl. Concentrations of RNG-U_5 and the oligonucleotides were determined spectrophotometrically from molar extinction coefficients [8600 M^{-1} cm^{-1} at 268 nm for poly(dA); 9350 M^{-1} cm^{-1} at 260 nm for poly(rU); 12,680 M^{-1} cm^{-1} at 268 nm for poly(rA); and 8220 M^{-1} cm^{-1} at 268 nm for poly(dT)]. For T_m denaturation, hyperchromicity was used. Data were recorded every 1 °C. Samples were covered with mineral oil to prevent evaporation. The reported T_m values are an average of three experiments (±0.2).

4.3. Circular dichroism spectra

CD spectra were obtained on an OLIS RSM circular dichroism spectrophotometer. Samples were held in a 1 cm path-length cuvette and maintained at 20 °C. Scans were run from 320 to 200 nm taking measurements every 1 nm. The integration time for each data point was 2 s. Ten scans were made of each sample, then averaged and smoothed using a 15 point exponential fitting algorithm.

4.4. Molecular dynamics setup

A detailed description of the MD setup, execution, and structural analysis is given in a previous report,[43] with a summary of methods presented here. The CHARMM27 all-atom nucleic acid residue topology and parameter files[44,45] were used for the DNA simulations, including counterions. Parameters for RNG were obtained based on similar structural groups found in amino acids (most notably arginine). The partial atomic charges[43] of the RNG backbone were evaluated with the CHelpG option (Breneman scheme) at the MP2/6-311+G(2d,p) level using Gaussian03.[46] The initial structures were constructed using QUANTA98,[47] selecting A-form as an initial conformer. Counterions (Na^+ and Cl^-) were added 5 Å away from each phosphorus or guanidinium carbon. These structures were energy minimized for 500 steps of steepest descent (SD) followed by 1000 steps of the adopted basis Newton–Raphson (ABNR) method using CHARMM (v. c27b4).[48]

4.5. MD details

The minimized systems were solvated in an orthorhombic box (45 Å × 64 Å × 44 Å) of pre-equilibrated TIP3P[49] water molecules, deleting solvent molecules that had an oxygen atom within 2.8 Å of a solute heavy atom. Periodic boundary conditions were applied. Images were generated using the CRYSTAL module of CHARMM. Electrostatic interactions were treated with the particle mesh Ewald method[50,51] using a real space cutoff of 10 Å. The solvent was minimized for 100 SD steps and 1000 ABNR steps while the solute was kept fixed. All constraints were then released and the entire system was minimized for 2000 ABNR steps. During dynamics, SHAKE[52] was used to constrain covalent bonds involving hydrogen atoms. The leapfrog-Verlet algorithm[53] was used for integration with a time-step of 1.5 fs. The solute and counterions were initially constrained while the solvent was allowed to equilibrate at 300 K under constant pressure and temperature. The constraints on the ions were then released, followed by those on the oligonucleotide, and the system was gradually heated to 300 K. After the heating period of 135 ps, the system continued to equilibrate for 365 ps under constant volume and temperature (NVT) conditions. Following this initial 500 ps heating and equilibration period, the production stage was carried out using the NVT ensemble until the total dynamics time reached 5 ns. Analyses involved the final 4.5 ns, with evaluations of sugar puckers, torsion angles, and intrastrand distances including the central 8 base-pairs of each oligomer. Helical parameters were determined by use of FREEHELIX,[54] evaluating the central 7 base-steps and 8 base-pairs of each dodecamer. Molecular representations were produced using Pymol.[55]

Acknowledgment

This work was supported by a grant from the National Institute of Health (DK09171).

References and notes

1. Uhlmann, E.; Peyman, A. *Chem. Rev.* **1990**, *90*, 543.
2. De Mesmaeker, A.; Haener, R.; Martin, P.; Moser, H. E. *Acc. Chem. Res.* **1995**, *28*, 366.

3. Agrawal, S.; Zhao, Q. Y. *Curr. Opin. Chem. Biol.* **1998**, *2*, 519.
4. Thoung, N. T.; Helene, C. *Angew. Chem. Int. Ed. Engl.* **1993**, *32*, 666.
5. Cook, P. D. *Nucleosides Nucleotides* **1990**, *18*, 1141.
6. Stein, C. A.; Cheng, Y.-C. *Science* **1993**, *261*, 1004.
7. Tseng, B. Y.; Ts'o, P. O. P. *Antisense Res. Dev.* **1995**, *5*, 251.
8. Morvan, F.; Sanghvi, Y. S.; Perbost, M.; Vasseur, J.-J.; Bellon, L. *J. Am. Chem. Soc.* **1996**, *118*, 255.
9. De Mesmaeker, A.; Lesueur, C.; Bevierre, M.-O.; Waldner, A.; Fritsch, V.; Wolf, R. M. *Angew. Chem. Int. Ed. Engl.* **1996**, *35*, 2790.
10. Bohler, C.; Nielsen, P. E.; Orgel, L. E. *Nature* **1995**, *376*, 578.
11. Veselkov, A. G.; Demidov, V. V.; Frank-Kamenetiskii, N. D.; Nielsen, P. E. *Nature* **1996**, *379*, 214.
12. Uhimann, E.; Peyman, A.; Breipohl, G.; Will, D. W. *Angew. Chem. Int. Ed. Engl.* **1998**, *37*, 2796.
13. Peyman, A.; Uhlmann, E.; Wagner, K.; Augustin, S.; Breipohl, G.; Will, D. W.; Schafer, A.; Wallmeier, H. *Angew. Chem. Int. Ed. Engl.* **1996**, *35*, 2636.
14. Fujii, M.; Yoshida, K.; Hidaka, J. *Bioorg. Med. Chem. Lett.* **1997**, *7*, 637.
15. Dempcy, R. O.; Browne, K. A.; Bruice, T. C. *J. Am. Chem. Soc.* **1995**, *117*, 6140.
16. Dempcy, R. O.; Browne, K. A.; Bruice, T. C. *Proc. Natl. Acad. Sci. U.S.A.* **1995**, *92*, 6097.
17. Dempcy, R. O.; Almarsson, O.; Bruice, T. C. *Proc. Natl. Acad. Sci. U.S.A.* **1994**, *91*, 7864.
18. Browne, K. A.; Dempcy, R. O.; Bruice, T. C. *Proc. Natl. Acad. Sci. U.S.A.* **1995**, *92*, 7051.
19. Linkletter, B. A.; Szabo, I. E.; Bruice, T. C. *J. Am. Chem. Soc.* **1999**, *121*, 3888.
20. Linkletter, B. A.; Szabo, I. E.; Bruice, T. C. *Bioorg. Med. Chem.* **2000**, *8*, 1893.
21. Linkletter, B. A.; Szabo, I. E.; Bruice, T. C. *Nucleic Acids Res.* **2001**, *29*, 2370.
22. Barawkar, D. A.; Bruice, T. C. *Proc. Natl. Acad. Sci. U.S.A.* **1998**, *95*, 11047.
23. Inoue, H.; Hayase, Y.; Imura, A.; Iwai, S.; Miura, K.; Ohtsuka, E. *Nucleic Acid Res.* **1987**, *15*, 6131.
24. Kojima, N.; Bruice, T. C. *Org. Lett.* **2000**, *2*, 81.
25. Kojima, N.; Szabo, I. E.; Bruice, T. C. *Tetrahedron* **2002**, *58*, 867.
26. Park, M.; Bruice, T. C. *Bioorg. Med. Chem. Lett.* **2005**, *15*, 3247.
27. Luo, J.; Bruice, T. C. *J. Am. Chem. Soc.* **1997**, *119*, 6693.
28. Huang, C. Y. *Method Enzymol.* **1982**, *87*, 509.
29. Szabo, I. E.; Bruice, T. C. *Bioorg. Med. Chem.* **2004**, *12*, 4233.
30. Marky, L. A.; Breslauer, K. J. *Biopolymers* **1987**, *26*, 1601.
31. Breslauer, K. J. In *Methods in Molecular Biology*, Agrawal, S., Eds.; Humana Press: Totowa, 1995; Vol. 26, p 347.
32. Kibler-Herzog, L.; Zon, G.; Uznanski, B.; Whittier, G.; Wilson, W. D. *Nucleic Acids Res.* **1991**, *19*, 2979.
33. Kandimalla, E. R.; Manning, A.; Zhao, Q.; Shaw, D. R.; Byrn, R. A.; Sasisekharan, V.; Agrawal, S. *Nucleic Acids Res.* **1997**, *25*, 370.
34. Cantor, C. R.; Fairclough, R. H.; Newmark, R. A. *Biochemistry* **1969**, *8*, 3610.
35. Johnson, W. C. In *Circular Dichroism and the Conformational Analysis of Biomolecules*, Fasman, G. D., Eds.; Plenum Press: New York, 1996; pp 433–468.
36. Gray, D. M.; Ratliff, R. L. *Biopolymers* **1975**, *14*, 487.
37. Gray, D. M.; Liu, J.-J.; Ratliff, R. L.; Allen, F. S. *Biopolymers* **1981**, *20*, 1337.
38. Gray, D. M.; Clark, C. L.; Cecil, P. K.; Singh, D. *Nucleic Acid Res.* **1997**, *25*, 4098.
39. Renisio, J.-G.; Cosquer, S.; Cherrak, I.; Antri, S. E.; Mauffret, O.; Fermandjian, S. *Nucleic Acids Res.* **2005**, *33*, 1970.
40. Conte, M. R.; Conn, G. L.; Brown, T.; Lane, A. N. *Nucleic Acids Res.* **1997**, *25*, 2627.
41. Calladine, C. R. *J. Mol. Biol.* **1982**, *161*, 343.
42. Willingham, A. P.; Orth, A. P.; Batalov, S.; Peters, E. C.; Wen, G. B.; Aza-Blank, P.; Hogenesch, J. B.; Shultz, P. G. *Science* **2005**, *309*, 1570.
43. Toporowski, J. W.; Reddy, S. Y.; Bruice, T. C. *Bioorg. Med. Chem.* **2005**, *13*, 3691.
44. MacKerell, A. D., Jr.; Bashford, D.; Bellott, M.; Dunbrack, R. L.; Evanseck, J. D.; Field, M. J.; Fischer, S.; Gao, J.; Guo, H.; Ha, S. *J. Phys. Chem. B* **1998**, *102*, 3586.
45. MacKerell, A. D.; Banavali, N. *J. Comput. Chem.* **2000**, *21*, 105.
46. Frisch, M. J.; Trucks, G. W.; Schlegel, H. B.; Scuseria, G. E.; Robb, M. A.; Cheeseman, J. R.; J.A. Montgomery, J.; Vreven, T.; Kudin, K. N.; Burant, J. C.; Millam, J. M.; Iyengar, S. S.; Tomasi, J.; Barone, V.; Mennucci, B.; Cossi, M.; Scalmani, G.; Rega, N.; Petersson, G. A.; Nakatsuji, H.; Hada, M.; Ehara, M.; Toyota, K.; Fukuda, R.; Hasegawa, J.; Ishida, M.; Nakajima, T.; Honda, Y.; Kitao, O.; Nakai, H.; Klene, M.; Li, X.; Knox, J. E.; Hratchian, H. P.; Cross, J. B.; Adamo, C.; Jaramillo, J.; Gomperts, R.; Stratmann, R. E.; Yazyev, O.; Austin, A. J.; Cammi, R.; Pomelli, C.; Ochterski, J. W.; Ayala, P. Y.; Morokuma, K.; Voth, G. A.; Salvador, P.; Dannenberg, J. J.; Zakrzewski, V. G.; Dapprich, S.; Daniels, A. D.; Strain, M. C.; Farkas, O.; Malick, D. K.; Rabuck, A. D.; Raghavachari, K.; Foresman, J. B.; Ortiz, J. V.; Cui, Q.; Baboul, A. G.; Clifford, S.; Cioslowski, J.; Stefanov, B. B.; Liu, G.; Liashenko, A.; Piskorz, P.; Komaromi, I.; Martin, R. L.; Fox, D. J.; Keith, T.; Al-Laham, M. A.; Peng, C. Y.; Nanayakkara, A.; Challacombe, M.; Gill, P. M. W.; Johnson, B.; Chen, W.; Wong, M. W.; Gonzalez, C.; Pople, J. A. Gaussian 03, Revision G.05; Gaussian, Inc.: Pittsburgh PA, 2003.
47. QUANTA98, Molecular Simulation Inc.: San Diego, CA, 1998.
48. Brooks, B. R.; Bruccoleri, R. E.; Olafson, B. D.; States, D. J.; Swaminathan, S.; Karplus, M. *J. Comput. Chem.* **1983**, *4*, 187.
49. Jorgensen, W. L.; Chandrasekhar, J.; Madura, J. D.; Impey, R. W.; Klein, M. L. *J. Chem. Phys.* **1983**, *79*, 926.
50. Darden, T.; York, D.; Pedersen, L. *J. Chem. Phys.* **1993**, *98*, 10089.
51. Petersen, H. G. *J. Chem. Phys.* **1995**, *103*, 3668.
52. Ryckaert, J. P.; Ciccotti, G.; Berendsen, H. J. C. *J. Comput. Phys.* **1997**, *23*, 237.
53. Verlet, L. *Phys. Rev.* **1967**, *159*, 98.
54. Dickerson, R. E. *Nucleic Acids Res.* **1998**, *26*, 1906.
55. Delano, W. L. "The PyMOL Graphics System." version 0.97, Delano Scientific LLC, San Carlos, CA, USA, 2004, http://www.pymol.org.